Submit to: Inorganic Chemistry

Nanostructured Ni_2SeS on Porous-Carbon Skeletons as Highly Efficient Electrocatalyst for Hydrogen Evolution in Acidic Medium

Yakun Tian[†,a], *Yuxi Zhang*[†,a], *Aijian Huang*[b,c], *Ming Wen**[,a], *Qingsheng Wu*[a], *Long Zhao*[a], *Mingkui Wang*[d], *Yan Shen*[d], *Zhiguo Wang**[,b], *Yongqing Fu*[e]

[a] School of Chemical Science and Engineering, Shanghai Key Laboratory of Chemical Assessment and Sustainability, Tongji University, 1239 Siping Road, Shanghai 200092, R. P. China.
[b] School of Electronics Science and Engineering, University of Electronic Science and Technology of China, Chengdu, 610054, P. R. China.
[c] Department of Chemistry, Tsinghua University, Beijing, 100084, China.
[d] Wuhan National Laboratory for Optoelectronics, Huazhong University of Science and Technology, Wuhan 430074, P. R. China
[e] Faculty of Engineering and Environment, Northumbria University, Newcastle upon Tyne, NE1 8ST, UK.

KEYWORDS

Nickel sulfoselenide, Porous nanostructure, Hydrogen Evolution Reaction, Electrocatalysis

ABSTRACT

Nickel dichalcogenides have received extensive attention as promising noble-metal-free nanocatalysts for hydrogen evolution reaction. Nonetheless, their catalytic performance is restricted by its sluggish reaction kinetics, limited exposed active sites and poor conductivity. In this work, we report on an effective strategy to solve those problems by using as-designed new porous-C/Ni_2SeS nanocatalyst which Ni_2SeS nanostubs anchored on porous-carbon skeletons process. Based on three advantages of the enhanced the intrinsic activity using the ternary sulfoselenide, increased number of exposed active sites due to the 3D hollow substrate, and increased conductivity caused by porous-carbon skeletons, the resulted porous-C/Ni_2SeS requires an overpotential of only 121 mV at a current density of 10 mA cm^{-2} with a Tafel slope of 78 mV dec^{-1} for hydrogen evolution in acidic media, and a good long-term stability. Density functional theory calculations also show that the Gibbs free energy of hydrogen adsorption of the Ni_2SeS is -0.23 eV, which is not only close to the ideal value (0 eV) and Pt reference (-0.09 eV), but is lower than NiS_2 and $NiSe_2$; Large electrical states exist in the vicinity of Fermi level, which further improve its electrocatalytic performance. This work provides new insights into rational design of ternary dichalcogenides and hollow structure materials for practical applications in HER catalysis and energy fields.

1. INTRODUTION

Hydrogen, as a clean green energy carrier, has been regarded as one of the alternatives to traditional energy, which can effectively improve climate change and address environmental problems.[1] In particular, hydrogen produced from water splitting has attracted extensive attention. The critical issue is the high-energy consumption of electric-energy to produce hydrogen from water which is related with the high electrolysis overpotential. The catalyst is one of the most important components for achieving the highly efficient electrochemical water splitting.[2-6] The most commonly used electrocatalysts for hydrogen evolution reaction (HER) are platinum (Pt) and its alloys which have critical issues such as low abundance and high cost. In the past few years, various materials such as transition metal carbides[7], nitrides[8], borides[9], sulfides[10], phosphides[11] and selenides[12], have been investigated as catalysts toward the electrochemical HER.[6,13] Among these, transition metal chalcogenides (TMCs) with a general formula of M_pX_q (M = transition metal, X = S, Se or Te) are especially attractive with good HER performances due to their large interlayer distances, tunable bandgaps, and transformable phases.[14,15] However, their limited exposed active sites, sluggish reaction kinetics and the poor conductivity restrict their successful applications as HER catalysts.

Currently there are three major strategies which have been proposed to optimize the HER catalytic performance of the TMCs: (i) improving the electrical conductivity; (ii) increasing the number of exposed active sites; (iii) enhancing the intrinsic activity of catalyst.[16] Correspondingly, there are three main methods to achieve these objectives. The first method is to use conductive nanomaterials as substrate to improve electron transfer within the HER electrocatalyst, such as carbonaceous materials.[17-20] The second method is to construct 3D nanostructures with large specific surface areas and make more active sites exposed. For example, recent studies have successfully synthesized nanostructured materials with preferentially exposed edge sites on the 3D nickel foam substrate, which has increased the catalytic activity due to more HER active sites exposed.[21-23] The third method is to introduce a third element to form ternary compounds to raise the intrinsic activity of catalyst (e.g. $Mo_{1-x}W_xSe_2$)[24,25]. With the addition of a third element, these ternary chalcogenides are very effective because of stoichiometric variations and synergistic effects compared to those of their binary counterparts.[26] Among them, numerous studies have been focused on using metal sulfoselenide as a substitute for HER. Ultrathin $MoS_{2(1-x)}Se_{2x}$ alloy nanoflakes were prepared and showed good activity and durability.[27] Ternary $CoS_{2x}Se_{2(1-x)}$ nanowire array was also synthesized and proved to be a stable electrode in the acidic media.[28] These results clearly show that partial anion-substitutions of transition metal sulfoselenide could achieve the desirable HER performance. Nevertheless, nickel sulfoselenide has been rarely studied in HER catalysis.

Based on the above the three methods and the good catalytic activity of Ni-based catalysts[29,30], in this study, we designed and developed porous-C/Ni_2SeS hollow structures with Ni_2SeS nanostubs (NSs) uniformly anchored onto the porous-carbon skeletons (PCSs)[31,32] as the highly effective electrocatalyst for the HER. Such a designed catalyst enable a superior HER performance with a low overpotential, a small Tafel slope and a long term stability. The as-prepared porous-C/Ni_2SeS hollow structures, when used as the catalyst, has three unique features which are beneficial for the electrocatalytic performance: (1) the PCSs supports ensure good conductivity of catalysts; (2) the as-designed 3D hollow PCSs have plentiful inter-connected macrochannels with large surface areas, which not only increase the number of Ni_2SeS exposed active sites and their effective availability in a unit volume with preventing the aggregation of nanostructures, but also improve the proton transport and catalytic velocity; (3) the ternary nickel sulfoselenide, compared with NiS_2 and $NiSe_2$, could enhance the intrinsic activity for HER. Density functional theory (DFT) calculations also reveal that the Gibbs free energy of hydrogen adsorption (ΔG_H) as a descriptor of HER indicates that Ni_2SeS show better catalytic performance than $NiSe_2$ and NiS_2. These results prove its potential as a new stable efficiency catalyst for HER.

2. EXPERIMENTAL DETAILS

2.1. Synthesis of porous-C/Ni_2SeS nanostructure

The porous-C/Ni_2SeS nanostructure was transformed from porous-C/$NiSe_2$ based on the PCSs synthesized from our previous works.[31,32] In a typical synthetic procedure, 1 mmoL $Ni(NO_3)_2 \cdot 6H_2O$, 0.5 mmoL selenium powder and 10 mg PCSs were added into 20 mL of distilled water at room temperature. The mixture was stirred for 30 min with ultrasonic treatment until the mixture was clear and the PCSs were dispersed homogeneously in the solution. Hydrazine hydrate solution (2 mL and 80% concentration) was then added into the solution, and the mixed solution were transferred to a 25 mL Teflon-lined stainless-steel autoclave, which was sealed and kept at 180°C for 24 hrs. After naturally cooled down to room temperature and washed with deionized water and ethanol, the product of porous-C/$NiSe_2$ was then dried in a vacuum dryer at 60°C for 4 hrs. Then the as-prepared porous-C/$NiSe_2$ composites (20 mg) and sulfur powders (500 mg) were put at two separate positions in two porcelain boats with sulfur powders at the upstream side of the furnace. Under N_2 atmosphere, the furnace temperature was increased from room temperature to 200°C, and from 200°C to 400 °C, with rate of 10°C min^{-1} and 2°C min^{-1}, respectively, and the composites were kept at 400 °C for 90 min. After naturally cooled down to room temperature, the final product of porous-C/Ni_2SeS was collected and washed with deionized water and ethanol for three times, and dried at 60°C for 4 hrs.

2.2. Characterization

Morphology and microstructures of the samples were investigated using a field emission scanning electron microscope (FE-SEM, JEOL, S-4800, Japan), a transmission electron microscope (TEM) and a high-resolution TEM (HRTEM, JEOL JEM-2100EX microscopy, Japan). X-Ray powder diffraction (XRD) patterns were recorded using a Bruker D8 advanced (German) diffractometer with a Cu Kα radiation source (γ=0.154056nm). Elemental maps were carried out under energy disperse X-ray spectroscopy (EDS) conducted at 15 keV on a TN5400 EDS instrument (Oxford). X-ray photoelectron spectroscopy (XPS) measurements were performed using a PHI-5000C ESCA system (Perkin Elmer) with Al Kα radiation (hv=1486.6 eV). The survey XPS spectrum (0-1100 eV) and high-resolution spectra were recorded using a RBD 147 interface XPS (RBD Enterprises, USA) and Auger Scan 3.21 software. Binding energies were calibrated using the containment carbon (C 1s=284.6 eV).

2.3. Electrochemical measurements

Electrochemical measurements were performed using an electrochemical workstation with a standard three-electrode setup (CH Instruments), with Ag/AgCl (in 3.5 M KCl solution) as the reference electrode, a graphite rod (Alfa Aesar, 99.9995%) as the counter electrode, and a glassy carbon electrode (GCE, 5 mm in diameter) coated with the as-prepared catalysts as the working electrode on a rotating disk electrode (RDE). All the measurements were carried out in 0.5 M H_2SO_4 aqueous solution and all the HER measurements were conducted in an N_2-saturated solution at ambient temperature. In a typical experiment, 4 mg of the catalyst was added in a mixture of 750 μL of water, 250 μL of ethanol and 40 μL of Nafion solution (5 wt%). The mixture was vigorously sonicated for about 30 min to form a homogeneous ink solution. Electrocatalyst suspension of 10 μL was dropped onto the glassy carbon electrode (with a mass loading of ~0.204 mg cm^{-2}). All the measurements were referred to the reversible hydrogen electrode (RHE) by using the relationship (eqn (1)):

$$E(RHE) = E(Ag/AgCl) + E_0(Ag/AgCl) + 0.059V \times pH \quad (1)$$

Linear sweep voltammetry (LSV) was used to examine the electrochemical activities of these samples at a scan rate of 5 mV s^{-1} with a RDE at 1600 rpm. Electrochemical impedance spectroscopy (EIS) measurements were carried out in the frequency range from 10^6 to 0.1 Hz with an overpotential of 150 mV. Additionally, chronoamperometry durability tests were conducted at 150 mV and cyclic voltammetry (CV) tests were performed for 300 cycles between -0.4 V and 0.2 V (vs. RHE) at 100 mV s^{-1} to investigate the electrochemical stability of the catalysts. All these results were calibrated by *iR* correction.

3. RESULTS and DISCUSSION

3.1. Microstructure analysis

As illustrated in Figure 1, the porous-C/Ni_2SeS hollow structures were synthesized through a solvothermal-chemical vapor deposition (CVD) process. Based on PCSs prepared by spray-pyrolysis (Figure S1), selenium powder and nickel nitrate hexahydrate are used as the Se and Ni resource, which was ultrasonicated with the PCSs to make Ni^{2+} and Se fully absorbed onto PCSs; After that, hydrazine hydrate solution was injected into the solution to form in situ reduced Se^{2-}. In the whole solvothermal reaction, there isn't Ni(0) due to its lower redox potential. Then, we employed a facile CVD method for further converting porous-C/$NiSe_2$ to porous-C/Ni_2SeS through sulfurization reaction.

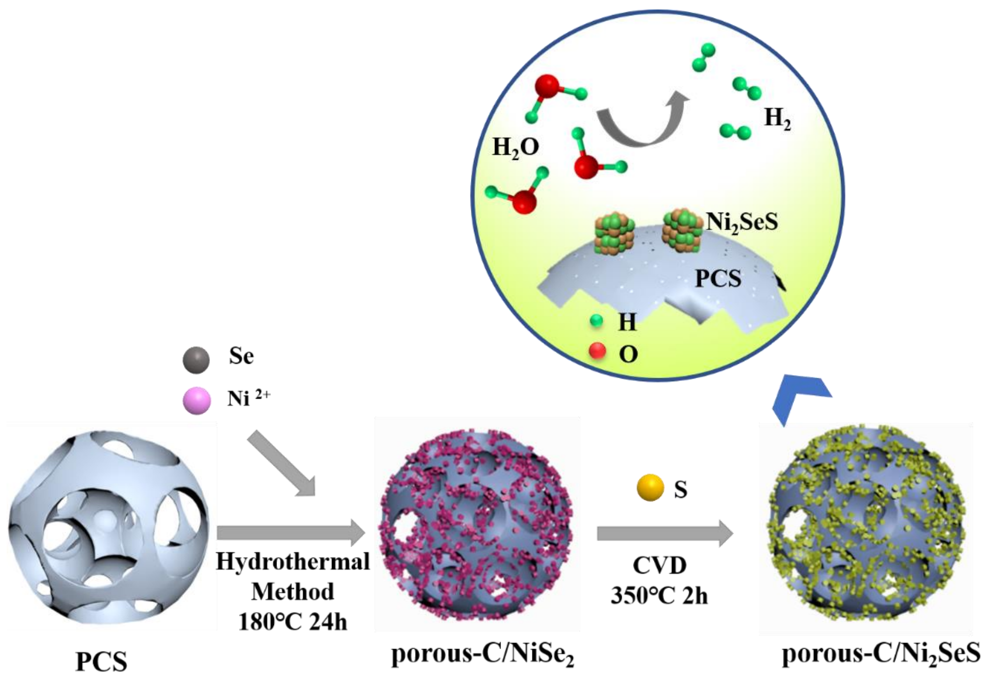

Figure 1 The schematic view of the formation and catalytic mechanism for porous-C/Ni_2SeS.

Figure 2 shows the morphology and microstructures of the synthesized porous-C/Ni_2SeS hollow structures. As shown in Figures 2A-C, the Ni_2SeS NSs are uniformly dispersed onto the surface of the PCSs. In addition, the constructed hollow 3D structure remains the porous structure of PCSs with abundant interconnected macropores. Compared to the structure of Ni_2SeS NSs without the PCSs (Figure S2), the newly formed hollow structures can increase specific surface areas and expose more active sites. Moreover, the Ni_2SeS NSs have a narrow distribution of crystal diameters within 6-14 nm (Figure 2D and the inset). In Figure 2E, the HRTEM image shows clear lattice fringes of 0.2667 nm and 0.2031 nm, which are responding to (101) and (102) plane of Ni_2SeS, respectively. The selected area electron diffraction (SAED) pattern in Figure 2F exhibits the polycrystalline diffraction rings, revealing the existence of tiny particle sizes relative to the electron beam spot.[33] A set of bright diffraction rings can be indexed to be the diffraction patterns of (220), (311), (400) and (440) planes, respectively. EDS elemental mapping images indicate that Ni, Se and S elements are uniformly distributed on PCSs (Figure 2G-J).

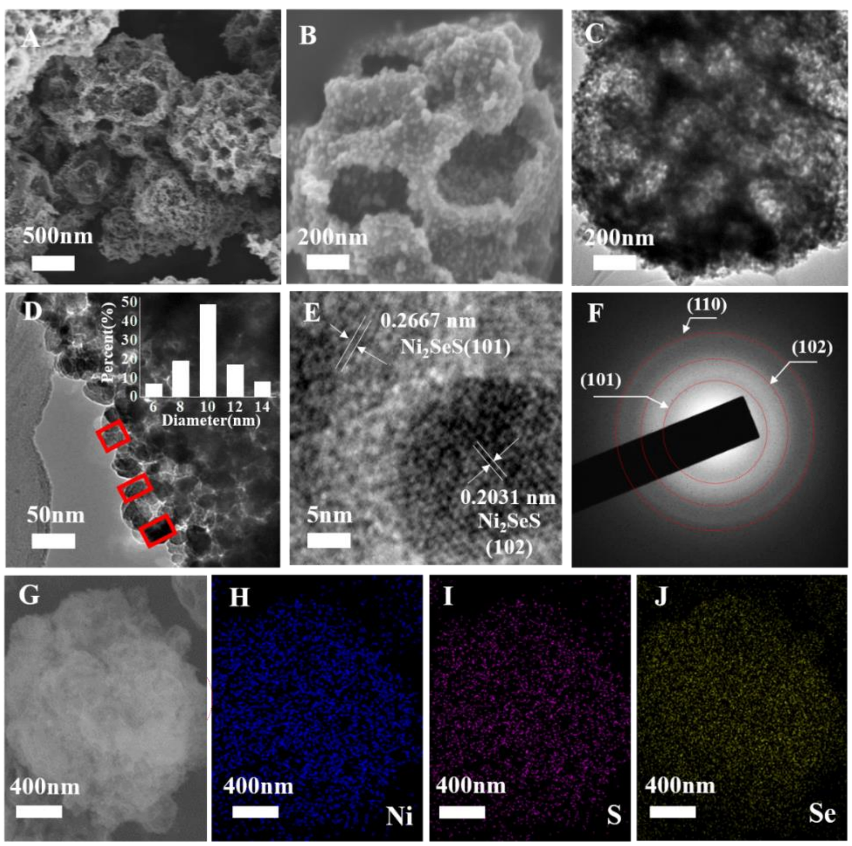

Figure 2 Morphology and structure characterization of porous-C/Ni_2SeS hollow structure: (A, B) SEM images and (C, D) TEM images (Inset: particle size distribution) with different magnification; (E) HRTEM image; (F) SAED image; (G-J) SEM-EDS elemental mapping.

Figure 3A shows XRD patterns of as-prepared products. Contrast to porous-C/NiS_2 (PDF# 11-0099) and porous-C/$NiSe_2$ (PDF# 65-1843), porous-C/Ni_2SeS presents four major peaks at 2θ values of 33.5, 44.8, 51.3, 62.7°, which can be indexed to the (101), (102), (110) and (112) planes of Ni_2SeS, respectively (PDF# 65-4017, Figure S2). This clearly demonstrates that the porous-C/Ni_2SeS has been converted from porous-C/$NiSe_2$ based on the amorphous structure of PCSs (Figure S1D). Figure 3B shows the EDS elemental analysis results. The porous-C/Ni_2SeS has an atomic ratio of Ni:Se:S at ~2:1:1, which indicates that it has an elemental stoichiometry of Ni_2SeS.

XPS analysis was further performed to acquire valence and elemental binding information of the porous-C/Ni_2SeS. In Figure 3C, the survey spectrum shows peaks of C 1s, O 1s, Ni 2p, S 2p and Se 3d in the binding energy region from 0 to 1100 eV. The high-resolution spectrum of Ni 2p could be fitted into four peaks (Figure 3D). Apart from the satellite peaks, two main peaks located at 852.6 and 870.7 eV are attributed to Ni $2p_{3/2}$ and $2p_{1/2}$, which are similar to those reported for Ni_3S_2, NiS and NiS_2.[34] The process giving rise to the Ni $2p_{3/2}$ peak is mainly of metal (Ni) character, with little contribution from the surrounding ligand.[35,36] Therefore, the nickel $2p_{3/2}$ peaks of porous-C/Ni_2SeS are very close in position to that of metallic nickel (852.5 ± 0.2 eV).[34,36] High resolution spectrum of S 2p signal is shown in Figure 3E. The doublet peaks of 161.9 (S $2p_{3/2}$) and 163.1 eV (S $2p_{1/2}$) are slightly lower than the reported spectra of nickel sulfides[34,36] because of the substitution of Se. In a similar way, the high resolution Se 3d peak can be split into two well-defined $3d_{5/2}$ and $3d_{3/2}$ peaks at 54.6 and 55.5 eV (Figure 3F), which is a negative shift of compared with nickel selenide [35,37] due to the substitution of S. What's more, the peak at around 58.7 eV is corresponding to the Se-O bonds, indicating the surface oxidation species of Se.[37] Thus, the below XPS results demonstrate the Ni_2SeS have been synthesized successfully on the PCSs.

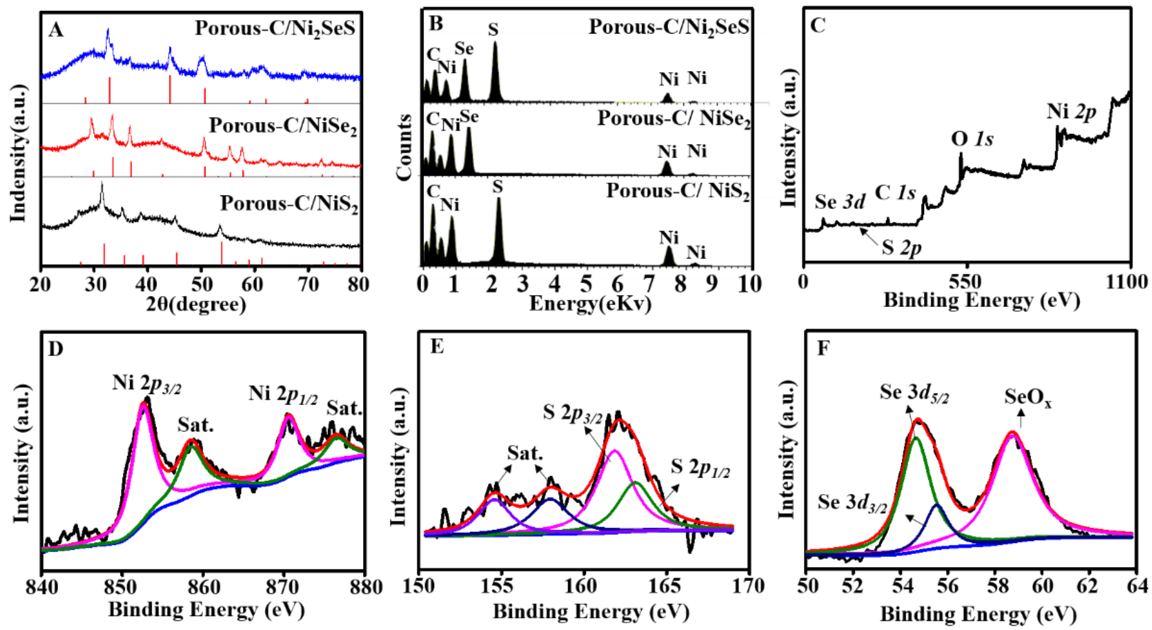

Figure 3 (A) XRD and (B) EDS patterns of the prepared samples; XPS analysis of (C) full spectra, (D) Ni 2p, (E) S 2p and (F) Se 3d of porous-C/Ni_2SeS.

3.2. Catalytic Performance

The LSV polarization curves and their values at 10 mA cm^{-2} of porous-C/Ni_2SeS and the control samples are shown in Figure 4A and C. The porous-C/Ni_2SeS exhibits improved electrocatalytic activity with 121 mV at 10 mA cm^{-2}, if compared with those of porous-C/NiS_2 (232 mV at 10 mA cm^{-2}) and porous-C/$NiSe_2$ (174 mV at 10 mA cm^{-2}). Such result is comparable with those of the previously reported MS_xSe_y materials, as summarized in Table S1. In addition, it demonstrates that the Ni_2SeS has an overpotential of 144 mV to reach the current density of 10 mA cm^{-2}, while those of NiS_2 (Figure S4A) and $NiSe_2$ (Figure S5A) have values of 245 and 194 mV, respectively. These results conclude that the ternary Ni sulfoselenide shows a better HER activity than its binary counterparts, which is verified in the following DFT calculations. Furthermore, the overpotentials of porous-C/Ni_2SeS, porous-C/NiS_2 (Figure S4B) and porous-C/$NiSe_2$ (Figure S5B) is lower than those of Ni_2SeS (144 mV at 10 mA cm^{-2}), NiS_2 and $NiSe_2$. The results clearly indicate that the substrate of PCSs plays an important role to improve the HER performance due to its unique interconnected channels and good conductivity.[31,32] The Tafel slope, which is derived from the polarization curve, is commonly used to discern the rate-determining step and the possible HER reaction pathway.[6] The linear portion of the Tafel plot was fitted using the conventional equation (eqn (2)):

$$\eta = b \log j + a \tag{2}$$

where η is the overpotential, j is the current density, and b is the Tafel slope. As shown in Figures 4B and C, the obtained results for the porous-C/Ni_2SeS show a Tafel slope of 78 mV per decade, which is smaller than those of porous-C/NiS_2 (142 mV per decade), porous-C/$NiSe_2$ (110 mV per decade), Ni_2SeS (99 mV per decade), NiS_2 (212 mV per decade) and $NiSe_2$ (141 mV per decade), As is well known, the HER in acidic electrolytes consists three reactions[38] (eqn (3)–(5)):

The discharge reaction or Volmer reaction:

$$H^+ + e^- \rightarrow H_{ad}^* \tag{1}$$

The electrochemical desorption reaction or Heyrovsky reaction:

$$H_{ad}^* + H^+ + e^- \rightarrow H_2 \tag{2}$$

The recombination reaction or Tafel reaction:

$$H_{ad}^* + H_{ad}^* \rightarrow H_2 \tag{3}$$

Theoretically, the Tafel slope is 118 mV per decade, 39 mV per decade or 29.5 mV per decade when reaction follow Volmer, Volmer-Heyrovsky and Volmer-Tafel mechanism.[6] Therefore, the porous-C/Ni_2SeS electrode follows the Volmer-Heyrovsky reaction mechanism and the migration of adsorbed hydrogen intermediate state (H_{ad}*) is the rate-limiting step in the overall HER process. EIS measurement results are shown in Figure 4D. The obtained charge-transport impedance (R_{ct})

of porous-C/Ni_2SeS is 51 Ω, which is lower than that of Ni_2SeS, suggesting that the interconnected porous structure of PCSs improves the proton transport and catalytic velocity.[39]

Figure 4E shows the characterization results of durability of Ni_2SeS and porous-C/Ni_2SeS, which is another important parameter for HER. Compared with those of Ni_2SeS, the Ni_2SeS NSs on PCSs possesses larger and more stable electric current densities at a static overpotential (150 mV). In particular, the polarization curve of porous-C/Ni_2SeS after 300 cycles is similar to that of the initial one (Figure 4F). These results clearly indicates that the insoluble and stable carbon supports have provided a high durability of the catalysts. After the chronoamperometry durability test, the large mass of Ni_2SeS were loaded onto the PCSs, suggesting an outstanding stability during the HER process (Figure S6).

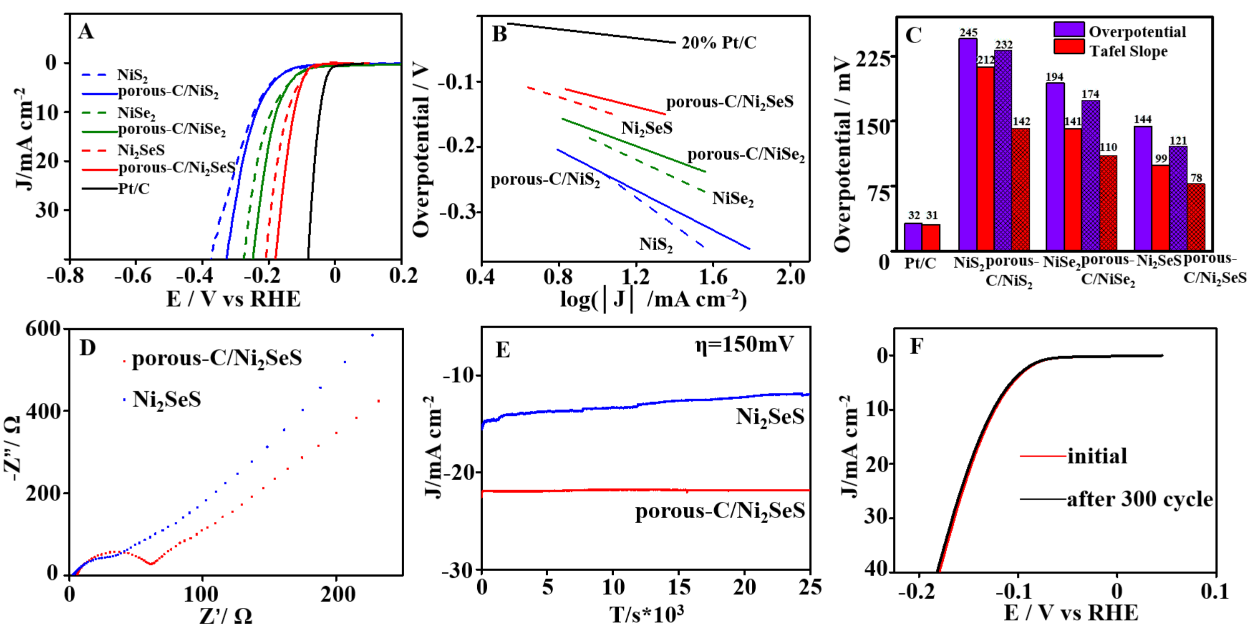

Figure 4 (A) Polarization curves, (B) Tafel plots, (C) the values of the overpotential at 10 mA cm^{-2} and Tafel slope, (D) Nyquist plots and (E) Chronoamperometry curves of the prepared samples; (F) Stability tests of porous-C/Ni_2SeS with initial polarization curve and the one after 300 potential cycles.

3.3. DFT calculations

In order to clarify the mechanism for the performance enhancement, we performed DFT calculations as implemented in the VASP codes[40], details of computation are given in the Supporting Information. The atomic structures of the bulk NiS_2, $NiSe_2$ and Ni_2SeS used in the DFT calculation are illustrated in Figure S7. Based on the previous part of synthesized NiS_2, $NiSe_2$, and Ni_2SeS, NiS_2 and $NiSe_2$ belong to the space group $Pa\overline{3}$, and theoptimized lattice constants are a = b = c = 5.63 Å for NiS_2 and a = b = c = 5.96 Å for $NiSe_2$ unti cell. Whereas the Ni_2SeS are in $P6_3/mmc$ space group and the calculated lattice constants are a=b= 3.57 Å, c= 5.27 Å. These lattice constants and crystal structures are well consistent with our experimental studies and other theoretical data[41,42]. In this study, the (001) surface of NiS_2 and $NiSe_2$ was investigated for HER performance. The possible adsorption sites of hydrogen absorbed on the surface are determined based on the symmetry of surface geometry (as shown in Figure S8). For example, there are two possible adsorption sites on NiS_2 (001) surface as show in Figure S8a: the top Ni sites (Ni) and top S sites (S). For Ni_2SeS, the (110) surface was selected to study its HER performance due to its regular atomic arrangement, and the Ni, S, Se sites are all exposed on these facets as shown in Figure S8c. Thus, six candidated H adsorption sites on the surface are take into account, including three surface sites (Ni1, S1 and Se1) and three hollow sites (Ni2, S2 and Se2).

According to thermodynamics, ΔG_H is a common descriptor for evaluating the HER performance. The ΔG_H should be close to zero for an ideal catalyst[43-45], in order to be beneficial for a faster formation of H_{ad}* and to provide a rapid concomitant hydrogen releasion. The HER free energy diagrams for different catalyst surface sites on NiS_2, $NiSe_2$ and Ni_2SeS are illustrated in Figure 5. For the (001) surface of NiS_2 (Figure 5A), the ΔG_H of Ni sites is -1.49 eV, which is too large for the hydrogen molecules releasion from the catalytic sites. Similar results are also obtained for the (001) surface of $NiSe_2$ as shown in Figure 5B. The ΔG_H of the surface Ni sites is -0.41 eV, which is much closer to zero than that on the NiS_2 surface, however, is still not good enough for the requirement of advanced HER catalyst.

The adsorption of H on the six possible sites on Ni_2SeS-(110) surface are also investigated, and the free energy diagrams of HER are shown in Figure 5C. The calculated Gibbs free energy for H adsorbed on hollow Se sites (Se2) is -0.23 eV, which is much close to the ideal value (0 eV) and Pt reference (-0.09 eV) than that of NiS_2 and $NiSe_2$.[46] These results exhibit the electrocatalytic performance of Ni_2SeS is better than NiS_2 and $NiSe_2$. Additionally, an ideal catalyst for HER reaction should also have good electron conductivity, the projected density of states (PDOS) for (001) surface of NiS_2, $NiSe_2$ and Ni_2SeS-(110) surface are shown in Figure S9. The PDOS results show continuous trend near the Fermi level, which are mainly composed of the Ni 3*d*, S 3*p* and Se 4*p* orbitals, revealing their intrinsically metallic features, faster rate of charge transfer. Therefore, on the basis of the results of our experimental and theoretical analysis based on the DFT calculations, we conclude that Ni_2SeS shows very good HER performance.

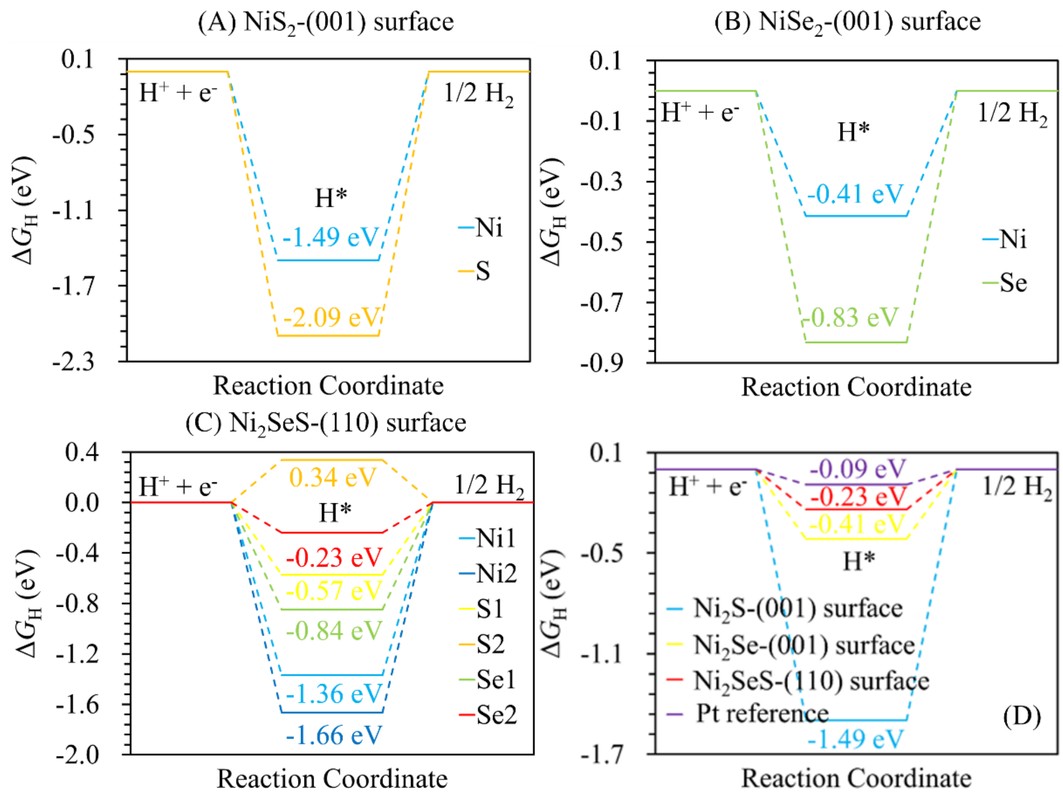

Figure 5 The ΔG_H diagram for H adsorbed on possible sites of (A) NiS_2-(001) surface, (B) $NiSe_2$-(001) surface, (C) Ni_2SeS-(110) surface and (D) summary of the ΔG_H on NiS_2, $NiSe_2$, Ni_2SeS and Pt reference at the condition of equilibrium potential and pH=0.

4. CONCLUSION

In summary, porous-C/Ni_2SeS, a ternary sulfoselenide based on 3D hollow structure, have been successfully synthesized via solvothermal and CVD methods. It shows superior HER electrocatalytic activity with a low overpotential of only 121 mV at a current density of 10 mA cm^{-2} with a Tafel slope of 78 mV dec^{-1}, as well as a good long-term durability, which is superior to those from the control groups of Ni_2SeS and porous-C/$NiSe_2$ or porous-C/NiS_2. Its excellent performances are caused by the following three reasons: (i) the better conductivity of the PCSs.; (ii) increasing the number of exposed active sites and specific surface areas due to the hollow structure; (iii) enhancing the intrinsic activity of catalyst by the ternary sulfoselenide system, which is consistent with the DFT calculation results. This study also provides new insights toward the design and improvement of new carbon-based ternary chalcogenides as a low cost and efficient catalyst electrode for water-splitting applications, and can be extended to design other Ni-based materials for high-performance HER catalysis.

ASSOCIATED CONTENT

Supporting Information

SEM images, XRD and EDS patterns. This material is available free of charge via the Internet at http://pubs.acs.org.

AUTHOR INFORMATION

Corresponding Author

* E-mail: m_wen@tongji.edu.cn; Fax: (+86) -21-65981097

Author Contributions

[†]These authors contributed equally to this work.

Notes

The authors declare no competing financial interest.

ACKNOWLEDGMENT

This work was financially supported by the National Natural Science Foundation of China (NSFC Nos: 21771140, 51271132, 91222103 and 11474047), Newton Mobility Grant (IE161019) through

Royal Society UK and NSFC and carried out at National Supercomputer Center in Tianjin, and the calculations were performed on TianHe-1(A).

REFERENCES

[1] Stamenkovic, V. R.; Strmcnik, D.; Lopes, P. P.; Markovic, N. M. Energy and fuels from electrochemical interfaces. *Nat. Mater.* **2017**, *16*, 57-69.

[2] Walter, M. G.; Warren, E. L.; McKone, J. R.; Boettcher, S. W.; Mi, Q. X.; Santori, E. A.; Lewis, N. S. Solar Water Splitting Cells. *Chem. Rev.* **2010**. *110*, 6446-6473.

[3] Zheng, Y.; Jiao, Y.; Jaroniec, M.; Qiao, S. Z. Advancing the Electrochemistry of the Hydrogen Evolution Reaction through Combining Experiment and Theory. *Angew. Chem. Int. Ed.* **2015**, *54*, 52-65.

[4] Morales-Guio, C. G.; Stern, L. A.; Hu, X. L. Nanostructured hydrotreating catalysts for electrochemical hydrogen evolution. *Chem. Soc. Rev.* **2014**, *43*, 6555-6569.

[5] Gordon, R. B.; Bertram, M.; Graedel, T. E. Metal stocks and sustainability. *Proc. Natl. Acad. Sci.* **2006**, *103*, 1209-1214.

[6] Zeng, M.; Li, Y. G. Recent advances in heterogeneous electrocatalysts for the hydrogen evolution reaction. *J. Mater. Chem. A* **2015**, *3*, 14942-14962.

[7] Chen, W. F.; Wang, C. H.; Sasaki, K.; Marinkovic, N.; Xu, W.; Muckerman, J. T.; Zhu, Y.; Adzic, R. R. Highly active and durable nanostructured molybdenum carbide electrocatalysts for hydrogen production. *Energy Environ. Sci.* **2013**, *6*, 943-951.

[8] Chen, W. F.; Muckerman, J. T.; Fujita, E. Recent developments in transition metal carbides and nitrides as hydrogen evolution electrocatalysts. *Chem. Commun.* **2013**, *45*, 8896-8909.

[9] Carenco, S.; Portehault, D.; Boissiere, C.; Mezailles, N.; Sanchez, C. Nanoscaled Metal Boride and Phosphides: Recent Developments and Perspectives. *Chem. Rev.* **2013**, *113*, 7981-8065.

[10] Li, Y. G.; Wang, H. L.; Xie, L. L.; Liang, Y. Y.; Hong, G. S.; Dai, H. J. MoS_2 Nanoparticles Grown on Graphene: An Advanced Catalyst for the Hydrogen Evolution Reaction. *J. Am. Chem. Soc.* **2011**, *133*, 7296-7299.

[11] Popczun, E. J.; McKone, J. R.; Read, C. G.; Biacchi, A. J.; Wiltrout, A. M.; Lewis, N. S.; Schaak, R. E. Nanostructured Nickel Phosphide as an Electrocatalyst for the Hydrogen Evolution Reaction. *J. Am. Chem. Soc.* **2015**, *135*, 9267-9270.

[12] Tang, H.; Dou, K.; Kaun, C. C.; Kuang, Q.; Yang, S. $MoSe_2$ nanosheets and their graphene hybrids: synthesis, characterization and hydrogen evolution reaction studies. *J. Mater. Chem. A* **2014**, *2*, 360-364.

[13] Yin, Y.; Zhang, Y. M.; Gao, T. L; Yao, T.; Zhang, X.; Han, J. C.; Wang, X.; Zhang, Z. H.; Xu, P.; Zhang, P.; Cao, X.; Song, B.; Jin, S. Synergistic Phase and Disorder Engineering in 1T-$MoSe_2$ anosheets for Enhanced Hydrogen-Evolution Reaction. *Adv. Mater.* **2017**, *29,* 1700311.

[14] Wang, Q.; Kalantar-Zadeh, K.; Kis, A.; Coleman, J. N.; Strano, M. S. Electronics and optoelectronics of two-dimensional transition metal dichalcogenides. *Nat. Nanotechnol.* **2012**, *7*, 699-712.

[15] Xu, J.; Zhang, J. J.; Zhang, W. J.; Lee, C. S. Interlayer Nanoarchitectonics of Two-Dimensional Transition-Metal Dichalcogenides Nanosheets for Energy Storage and Conversion Applications. *Adv. Energy Mater.* **2017**, *7*, 1700571.

[16] Seh, Z. W.; Kibsgaard, J.; Dickens, C. F.; Chorkendorff, I.; Nørskov, J. K.; Jaramillo, T. F. Combining theory and experiment in electrocatalysis: Insights into materials design. *Science* **2017**, *355*, 6321; Xu, C.; Peng, S. J.; Tan, C. L.; Ang, H. X.; Tan, H. T.; Zhang, H.; Yan, Q. Y. Ultrathin S-doped $MoSe_2$ nanosheets for efficient hydrogen evolution; *J. Mater. Chem. A* **2014**, *2*, 5597-5601.

[17] Li, D. J.; Maiti, U. N.; Lim, J.; Choi, D. S.; Lee, W. J.; Oh, Y.; Lee, G.; Kim, S. O. Molybdenum Sulfide/N-Doped CNT Forest Hybrid Catalysts for High Performance Hydrogen Evolution Reaction. *Nano Lett.* **2014**, *14*, 1228-1233.

[18] Liang, Q. H.; Zhong, L.; Du, C. F.; Zheng, Y.; Luo, Y. B.; Xu, J. W.; Li, S. Z.; Yan, Q. Y. Mosaic-Structured Cobalt Nickel Thiophosphate Nanosheets Incorporated N-doped Carbon for Efficient and Stable Electrocatalytic Water Splitting. *Adv. Funct. Mater.* **2018**, *28*, 1805075.

[19] Suo, L. Y.; Zhu, J. H.; Shen, X. Y.; Wang, Y. Z.; Han, X.; Chen, Z. Q.; Li, Y.; Liu, Y. R.; Wang, D.; Ma, Y. W. Hard carbon spheres interconnected by carbon nanotubes as high-performance anodes for sodium-ion batteries. *Carbon* **2019**, *151*, 1-9.

[20] He, P. G.; Ding, Z. P.; Zhao, X. D.; Liu, J. H.; Huang, Q.; Peng, J. J.; Fan, L. Z. Growth of carbon nanosheets on carbon nanotube arrays for the fabrication of three-dimensional micro-patterned supercapacitors. *Carbon* **2019**, *155*, 453-461.

[21] Chen, G. B.; Wang, T.; Zhang, J.; Liu, P.; Sun, H. J.; Zhuang, X. D.; Chen, M.; Feng, X. L. Accelerated hydrogen evolution kinetics on NiFe-layered double hydroxide electrocatalysts by tailoring water dissociation active sites. *Adv. Mater.* **2018**, *30*, 1706279.

[22] Du, F.; Shi, L.; Zhang, Y. T.; Li, T.; Wang, J. L.; Wen, G. H.; Alsaedi, A.; Hayat, T.; Zhou, Y.; Zou, Z. G. Foam-like Co_9S_8/Ni_3S_2 heterostructure nanowire arrays for efficient bifunctional overall water–splitting. *Appl. Catal., B* **2019**, *253*, 246-252.

[23] Yang, Y. Q.; Zhang, W. B; Xiao, Y.; Sh, Z.; Cao, X. M.; Tang, Y.; Gao, Q. S. $CoNiSe_2$ heteronanorods decorated with layered-double-hydroxides for efficient hydrogen evolution. *Appl. Catal., B* **2019**, *242*, 132-139.

[24] Liu, T. T.; Asiri, A. M.; Sun, X. P. Electrodeposited Co-doped $NiSe_2$ nanoparticles film: a good electrocatalyst for efficient water splitting. *Nanoscale* **2016**, *8*, 3911-3915.

[25] Meiron, O. E., Kuraganti, V.; Hod, I.; Bar-Ziv, R.; Bar-Sadan, M. Improved catalytic activity of $Mo_{1-x}W_xSe_2$ alloy nanoflowers promotes efficient hydrogen evolution reaction in both acidic and alkaline aqueous solutions. *Nanoscale* **2017**, *9*, 13998-14005.

[26] Gao, T.; Zhang, Q.; Li, L.; Zhou, X.; Li, L. G.; Li, H. Q.; Zhai, T. Y. 2D Ternary Chalcogenides. *Adv. Optical Mater.* **2018**, *6,* 1800058.

[27] Gong, Q. F.; Cheng, L.; Liu, C. H.; Zhang, M.; Feng, Q. L.; Ye, H. L.; Zeng, M.; Xie, L. M.; Liu, Z.; Li, Y. G. Ultrathin $MoS_{2(1-x)}Se_{2x}$ Alloy Nanoflakes For Electrocatalytic Hydrogen Evolution Reaction. *ACS Catal.* **2015**, *5*, 2213-2219.

[28] Liu, K. L.; Wang, F. M.; Xu, K.; Shifa, T. A.; Cheng, Z. Z.; Zhan, X. Y.; He, J. $CoS_{2x}Se2_{(1-x)}$ nanowire array: an efficient ternary electrocatalyst for the hydrogen evolution reaction. *Nanoscale* **2016**, *8,* 4699-4704.

[29] Gong, M.; Wang, D. Y.; Chen, C. C.; Hwang, B. J.; Dai, H. J. A mini review on nickel-based electrocatalysts for alkaline hydrogen evolution reaction. *Nano Res.* **2016**, *9*, 28-46.

[30] Ning, L.; Liao, S. Y.; Li, H.; Tong, R.; Dong, C. Q.; Zhang, M.; Gu, W.; Liu, X. Carbon-based materials with tunable morphology confined Ni (0) and $Ni\text{-}N_x$ active sites: Highly efficient selective hydrogenation catalysts; *Carbon* **2019**, *154*, 48-57.

[31] Chen, S. P.; Wu, Q. N.; Wen, M.; Wu, Q. S.; Li, J. Q.; Cui, Y.; Pinna, N.; Fan, Y. F.; Wu, T. Sea-Sponge-like Structure of Nano-Fe_3O_4 on Skeleton-C with Long Cycle Life under High Rate for Li-Ion Batteries, ACS *Appl. Mater. Interfaces* **2018**, *10*, 19656-19663.

[32] Chen, S. P.; Xing, K.; Wen, J. H.; Wen, M.; Wu, Q. S.; Cui, Y. Hierarchical assembly and superior sodium storage properties of a sea-sponge structured C/SnS@C nanocomposite. *J. Mater. Chem. A* **2018**, *6*, 7631-7638.

[33] Fang, H.; Wen, M.; Chen, H. X.; Wu Q. S.; Li, W. Y. Graphene stabilized ultra-small CuNi nanocomposite with high activity and recyclability toward catalysing the reduction of aromatic nitro-compounds. *Nanoscale* **2016**, *8*, 536-542.

[34] Jiang, N.; Tang, Q.; Sheng, M. L.; You, B.; Jiang, D.; Sun, Y. Nickel sulfides for electrocatalytic hydrogen evolution under alkaline conditions: a case study of crystalline NiS, NiS_2, and Ni_3S_2 nanoparticles. *Catal. Sci. Technol.* **2016**, *6*, 1077-1084.

[35] Tang, C.; Cheng, N.; Pu, Z.; Xing, W.; Sun, X. P. NiSe Nanowire Film Supported on Nickel Foam: An Efficient and Stable 3D Bifunctional Electrode for Full Water Splitting. *Angew. Chem. Int. Ed.* **2015**, *54*, 9351-9355

[36] Jiang, N.; Bogoev, L.; Popova, M.; Gul, S.; Yanob, J.; Sun, Y. J. Electrodeposited nickel-sulfide films as competent hydrogen evolution catalysts in neutral water. *J. Mater. Chem. A* **2016**, *2*, 19407-19414.

[37] Zhang, F. F.; Pei, Y.; Ge, Y.; Chu, H.; Craig, S.; Dong, P.; Cao, J.; Ajayan, P. M.; Ye, M.; Shen, J. F. Controlled Synthesis of Eutectic NiSe/Ni_3Se_2 Self-Supported on Ni Foam: An Excellent Bifunctional Electrocatalyst for Overall Water Splitting. *Adv. Mater. Interfaces* **2018**, *5*, 1701507.

[38] L. McCrory, C. C.; Jung, S. H.; Peters, J. C.; Jaramillo, T. F. Benchmarking Heterogeneous Electrocatalysts for the Oxygen Evolution Reaction. *J. Am. Chem. Soc.* **2013**, *135*, 16977–16987.

[39] Huang, J.; Xu, Z. L.; Abouali, S.; Garakani, M. A.; Kim, J. K. Porous graphene oxide/carbon nanotube hybrid films as interlayer for lithium-sulfur batteries. *Carbon* **2016**, *99*, 624-632.

[40] Kresse, G.; Furthmiiller, J. Efficiency of ab-initio total energy calculations for metals and semiconductors using a plane-wave basis set. *Computational Materials Science* **1996**, *6*, 15-50.

[41] Zhang, Y.; Jin, Z. Boosting Photocatalytic Hydrogen Evolution Achieved by NiS_x Coupled with g-C_3N_4@ZIF-67 Heterojunction. *J. Phys. Chem.* **2019**, *123*, 18248-18263.

[42] Du, S.; Li, C.; Lin, X.; Xu, W.; Huang, X.; Xu, H.; Fang, P. $NiSe_2$ as Co-Catalyst with CdS: Nanocomposites for High-Performance Photodriven Hydrogen Evolution under Visible‐Light Irradiation. *ChemPlusChem* **2019**, *84*, 999-1010.

[43] Greeley, J.; Jaramillo, T. F.; Bonde, J.; Chorkendorff, I. B.; Norskov, J. K. Computational high-throughput screening of electrocatalytic materials for hydrogen evolution. *Nat. Mater*. **2006**, *5*, 909-913.

[44] Jiao, Y.; Zheng, Y.; Jaroniec, M.; Qiao, S. Z. Design of electrocatalysts for oxygen- and hydrogen-involving energy conversion reactions. *Chem. Soc. Rev.* **2015**, *44*, 2060-2086.

[45] Nørskov, J. K.; Bligaard, T.; Logadottir, A.; Kitchin, J. R.; Chen, J. G.; Pandelov, S.; Stimming, U. Response to "Comment on 'Trends in the Exchange Current for Hydrogen Evolution' [J. Electrochem. Soc., 152, J23 (2005)]". *J. Electrochem. Soc.* **2006**, *153*, L33.

[46] Nørskov, J. K.; Bligaard, T.; Logadottir, A.; Kitchin, J. R.; Chen, J. G.; Pandelov, S.; Stimming, U. Trends in the Exchange Current for Hydrogen Evolution. *J. Electrochem. Soc.* **2005**, *152*, J23.

Table of Contents

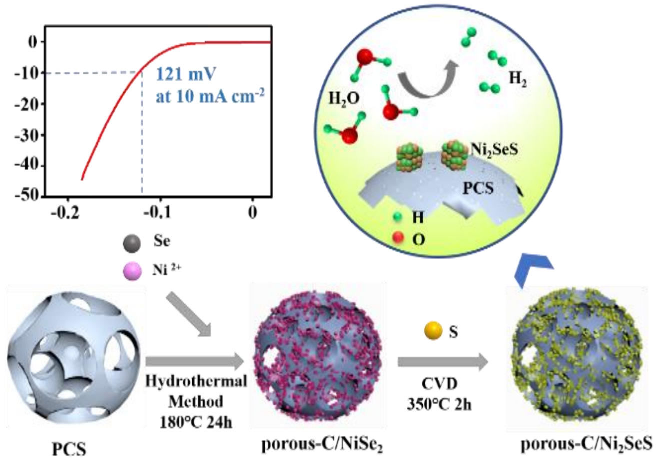

The porous-C/Ni_2SeS, based on its enhanced the intrinsic activity, increased number of exposed active sites, and increased conductivity, shows superior hydrogen evolution electrocatalytic activity.